Electronic Supplementary Material (ESI) for ChemComm.
This journal is © The Royal Society of Chemistry 2019

Supporting Information

Fe3O4-Encapsulated N-Doped Porous Carbon as Efficient Oxygen Reduction Reaction Electrocatalysts for Zn-Air Batteries

Longbin Li[a,b], Yizhe Li[a,b], Yingbo Xiao[a,b], Rong Zeng[a,b], Xiannong Tang[a,b], Weizu Yang[a,b], Jun Huang[a,b], Kai Yuan[a,b], Yiwang Chen*[a,b]*

[a.] College of Chemistry, Nanchang University, 999 Xuefu Avenue, Nanchang 330031, China.

[b.] Institute of Polymers and Energy Chemistry (IPEC), Nanchang University, 999 Xuefu Avenue, Nanchang 330031, China.

Corresponding author: E-mail addresses: kai.yuan@ncu.edu.cn (K. Yuan.), ywchen@ncu.edu.cn (Y. Chen.).

Experimental Section

Chemical Reagents and Materials. Pyrrole and polyvinyl alcohol (PVA) were obtained from TCI. Anhydrous $FeCl_3$ and Pt/C (20 wt% Pt) were obtained from Alfa Aesar. KOH and H_2SO_4 (98%) were purchased from Sinopharm Chemical Reagent Co. Ltd (China). Carbon paper was obtained from Hesen Electric Inc. Shanghai, and carbon cloth substrate was obtained from WOS 1002, CeTech.

Synthesis of GO-PPy@$FeCl_3$. First, a modified Hummer's method was used to prepare graphene oxide (GO).[65] Then, 50 mg of GO was dispersed in 180 mL of distilled (DI) water mixed with 20 ml of ethanol followed by sonication and vigorous stirring for 15 min. Subsequently, 120 mL of 0.276 M $FeCl_3$ solution was dropwise added under continuous stirring at room temperature for 24 h. The resulting product GO-PPy was obtained by filtration and washed with DI water repeatedly. GO-PPy was then dispersed in different certain concentrations of $FeCl_3$ solutions (with the pyrrole to $FeCl_3$ ratios of 6:1, 4:1, and 2:1), followed by rotary evaporation, and the obtained sample was named GO-PPy@$FeCl_3$.

Synthesis of 2D-FeNC. GO-PPy@$FeCl_3$ was carbonized at 800 °C for 2 h under N_2 atmosphere with a heating rate of 5 °C min^{-1} to obtain 2D-FeNC. For comparison, 2D-NC was also obtained without addition of $FeCl_3$ solution.

Synthesis of 2D-FeNC-KOH-*T*. First, 2D-FeNC were activated with KOH at different activation temperatures (600, 700, and 800 °C). After activation at different temperatures, and followed by leached in 0.5 M H_2SO_4 solution for 8 h at 80 °C, 2D-FeNC was converted into activated Fe,N codoped porous carbons (2D-FeNC-KOH-*T*), where *T* represents the temperature,

T= 600, 700, and 800. During the activation process, the mass ratio for 2D-FeNC to KOH was 1:4. For comparison, 2D-NC was also activated with KOH at 700 °C to fabricated 2D-NC-700.

Synthesis of 2D-Fe_3O_4@FeNC-*T*. The as-obtained samples were heated for a second time under N_2 atmosphere at 600 °C for 2 h to afford hybrid carbon nanosheets with Fe_3O_4 nanoparticles encapsulated in Fe,N codoped porous carbon (2D-Fe_3O_4@FeNC-*T,* *T*= 600, 700, 800) electrocatalysts.

Materials Characterizations. SEM measurements were performed via a Quanta 200F environmental scanning electron microscope (JEOL JSM-6380LV). TEM images, HRTEM images, SAED patterns, EDS and HAADF-STEM were performed by a scanning transmission electron microscope (JEOL, JEM-2100F). The nitrogen adsorption-desorption measurements were performed on an ASAP 2460 (MIC America Inc.), and the surface areas were obtained by the BET model. XRD patterns were obtained by a Bruker D8 Advance X-ray diffractometer. Raman spectroscopy was performed on a HORIBA Scientific LabRAM HR Raman spectrometer system. XPS spectra were recorded on a Kratos AXIS Ultra. For X-band Electron Paramagnetic Resonance Spectroscopy (EPR) measurements, the X-band (9.4 GHz) EPR spectrum were recorded at 298 K with a modulation amplitude of 1 mT and a modulation frequency of 100 kHz under argon atmosphere at 298K. ^{57}Fe Mößbauer measurements were recorded at 298K with a CMCA-550 (Wissel) with a ^{57}Co/Pd-source.

Oxygen Reduction Reaction (ORR) Reasurements. In this study, all the electrochemical measurements were tested by using a three-electrode cell system, and received from an

electrochemical workstation (AutoLab, PGSTAT302Nl). A rotating disk electrode (RDE) or rotating ring-disk electrode (RRDE) (Pine Research Instrumentation, USA) coated with the electrocatalyst was served as working electrode. A graphite rod and an Ag/AgCl electrode (3M KCl) were used as counter electrode and reference electrode, respectively. The electrolyte was 0.1 M KOH aqueous solution.

Preparation of the Working Electrode. First, 10 mg of the sample powder was mixed with 950 μL of ethanol and 50 μL of 5% wt% Nafion solution and sonicated for 30 min to obtain homogeneous catalyst ink. Next, 12 μL of the catalyst dispersion was pipetted onto a glassy carbon surface with a diameter of 5 mm. For comparison, the Pt/C catalyst slurry was obtained by the same procedure. Subsequently, 5 μL of the as-prepared catalyst dispersion were loaded for measurements. Finally, the electrodes were dried slowly under room temperature until a homogeneous catalyst film on the electrode surface was formed.

CV and RDE Measurements. CV experiments were collected at a scan rate of 20 mV/s between -0.95 and 0.05 V *vs*. Ag/AgCl. The RDE experiments were conducted at a scan rate of 10 mV/s under different rotating speeds. O_2 or N_2 was purged into the cell for 30min before the measurements and maintained during the experiments to insure O_2 or N_2 saturated in electrolyte. The potential measured in this study are aligned to reversible hydrogen electrode (RHE) scale by using the Nernst equation from Ag/AgCl.

$$E_{RHE} = E_{Ag/AgCl} + 0.059\text{pH} + E^{\theta}_{Ag/AgCl} \quad (1)$$

where $E_{Ag/AgCl}$ was the measured potential using Ag/AgCl, and $E^{\theta}_{Ag/AgCl}$, the standard potential of Ag/AgCl, was 0.1976 V.

The number of electrons transferred (n) and kinetic current density (J_K) for ORR can be determined from the Koutecky-Levich equation:

$$\frac{1}{J}=\frac{1}{J_L}+\frac{1}{J_K}=\frac{1}{B\omega^{1/2}}+\frac{1}{J_K} \quad (2)$$

$$B=0.62nFC_0(D_0)^{2/3}\nu^{-1/6} \quad (3)$$

$$J_K=nFkC_0 \quad (4)$$

where J, J_K and J_L are the experimentally measured, kinetic and diffusion limiting current densities, respectively, ω is the angular velocity of the rotating electrode (ω= 2πN, N is the linear rotation speed), n is the electron transfer number, k is the electron transfer rate constant, F is the Faraday constant (F= 96485 C mol^{-1}), D_0 is the diffusion coefficient of O_2 in 0.1 M KOH (1.9×10^{-5} cm^2 s^{-1}), C_0 is the bulk concentration of O_2 in the electrolyte (1.2×10^{-3} M), and v is the kinematic viscosity (0.01 cm^2 s^{-1}).

RRDE Measurements. Preparation of working electrodes was using the same procedure above. The constant ring potential was set at 0.5 V *vs*. Ag/AgCl during the measurements to oxide intermediates of ORR. According to the results of RRDE experiments, the HO_2^-(%) and the n values can be obtained by the following equations:

$$n=\frac{4I_{Disk}}{I_{Disk}+I_{Ring}/N} \quad (5)$$

$$\%(HO_2^-)=\frac{200\times I_{Ring}}{I_{Disk}+I_{Ring}/N} \quad (6)$$

where I_{Disk} and I_{Ring} are Faradaic disk and ring current, respectively. and the current collection efficiency of the Pt ring (N) was provided with a value of 0.37.

Liquid Zn-Air Battery Assembly. A homemade liquid Zn-air battery was fabricated for the evaluation of battery performance. It was constructed by pairing 2D-Fe_3O_4@FeNC-700 loaded onto a carbon paper with a Zn plate (0.20 mm thickness) in 6 M KOH. The batteries were organized via the following procedure: First, the air electrodes were prepared by pipetting catalyst slurry carefully onto the carbon paper (1.25 mg cm^{-2}) with the help of pipette. Subsequently, polished zinc plates were served as the anode. Batteries tests were carried out at room temperature under ambient atmosphere with a CHI 760E and a LAND CT2001A. The specific capacity and energy density can be obtained from the consumed Zn (gently polished and ultrasonically washed several times to remove byproducts or Zn dendrites) after discharge.

Flexible All-solid-state Zn-Air Battery Assembly. The air electrodes were prepared by pipetting catalyst slurry carefully onto the carbon cloth (2.50 mg cm^{-2}), while the anode was made by a polished Zn plate (0.10 mm thickness). The PVA/KOH was synthesized as follows: 1.0 g of PVA powder was mixed in 10.0 mL of DI water under continuous stirring at 95 °C for 2.0 h. Subsequently, 1.0 mL of 18.0 M KOH was dropwise added to the above mixed solution and the obtained gel was continuous stirred at same temperature for 40 min. Finally, PVA gel was sandwiched between the Zn plate and the as-prepared air electrode to assemble the flexible all-solid-state Zn-air battery.

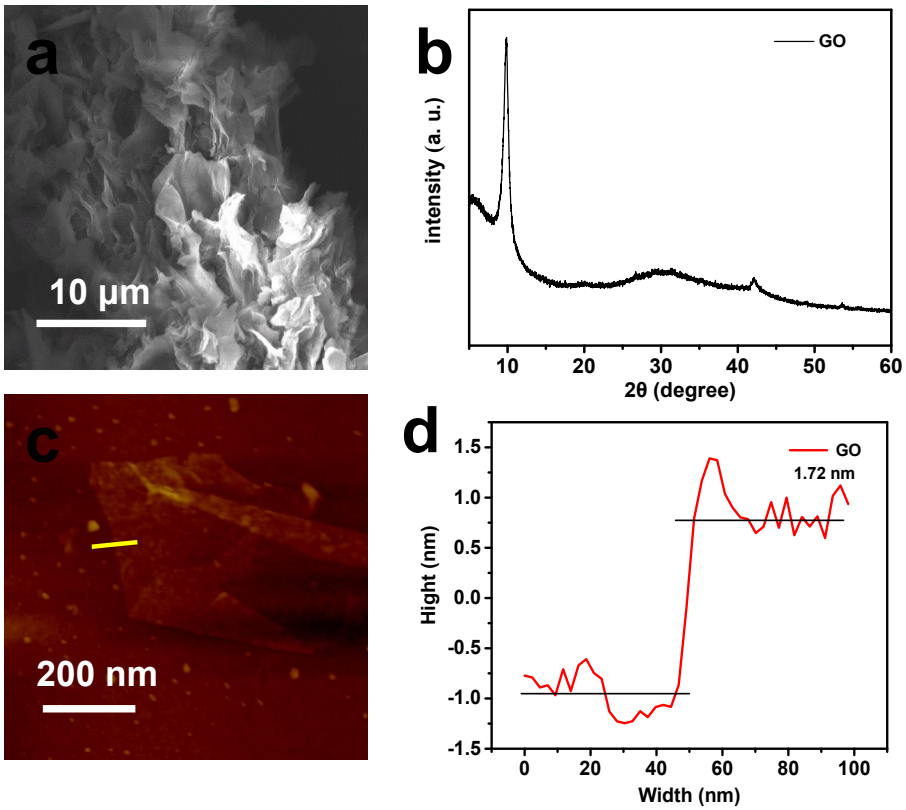

Fig. S1. (a) SEM image, (b) the XRD pattern, (c) AFM image and (d) corresponding height profile of GO. The AFM image and the corresponding height of GO showed, to further demonstrated, GO was identified by X-ray diffraction (XRD) patterns, and the GO shows an intense (002) peak centered at $2\theta = 11.3°$.

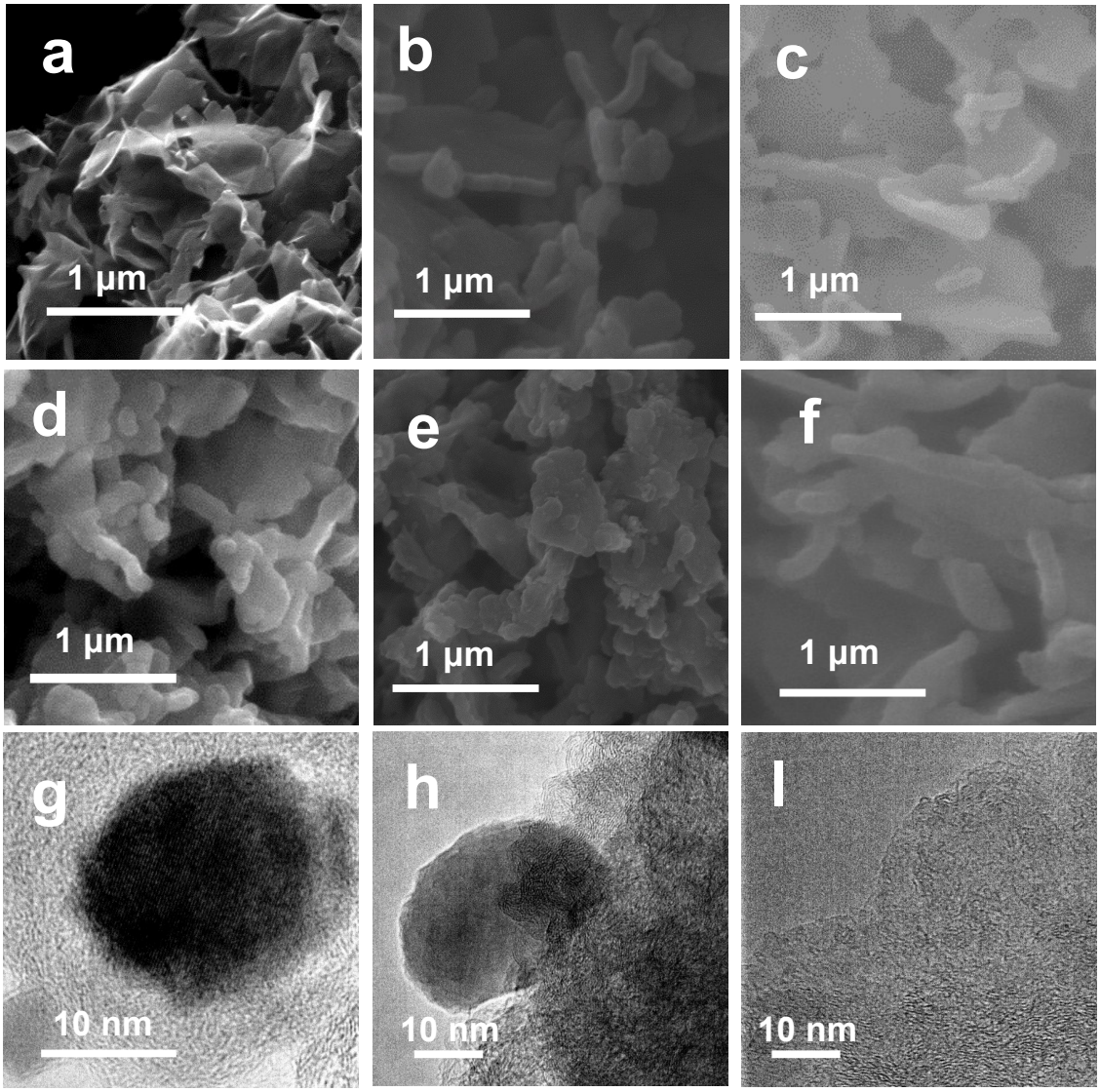

Fig. S2. SEM images of (a) GO, (b) GO-PPy, (c) 2D-FeNC; (d) 2D-Fe_3O_4@FeNC-600, (e) 2D-Fe_3O_4@FeNC-800, and (f) 2D-NC-700; HRTEM images of (g) 2D-Fe_3O_4@FeNC-600, (h) 2D-Fe_3O_4@FeNC-800, and (i) 2D-NC-700.

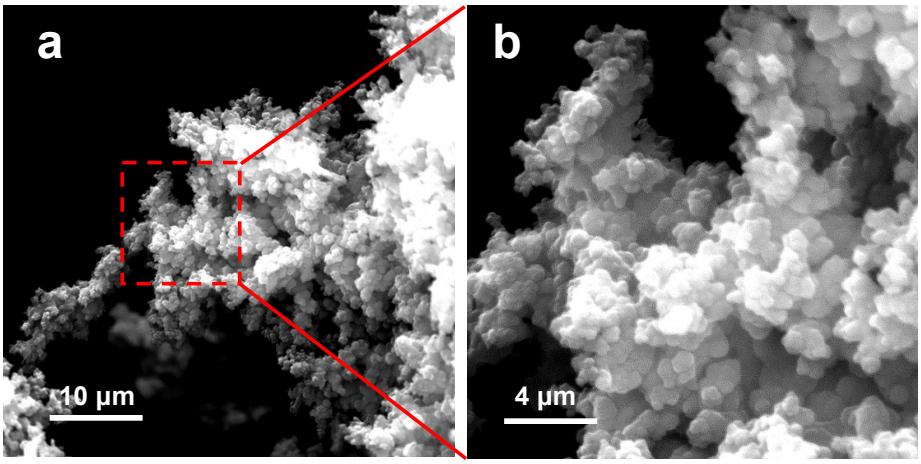

Fig. S3. (a) SEM image of Fe_3O_4@FeNC-700, (b) the right is an corresponding enlarged SEM image.

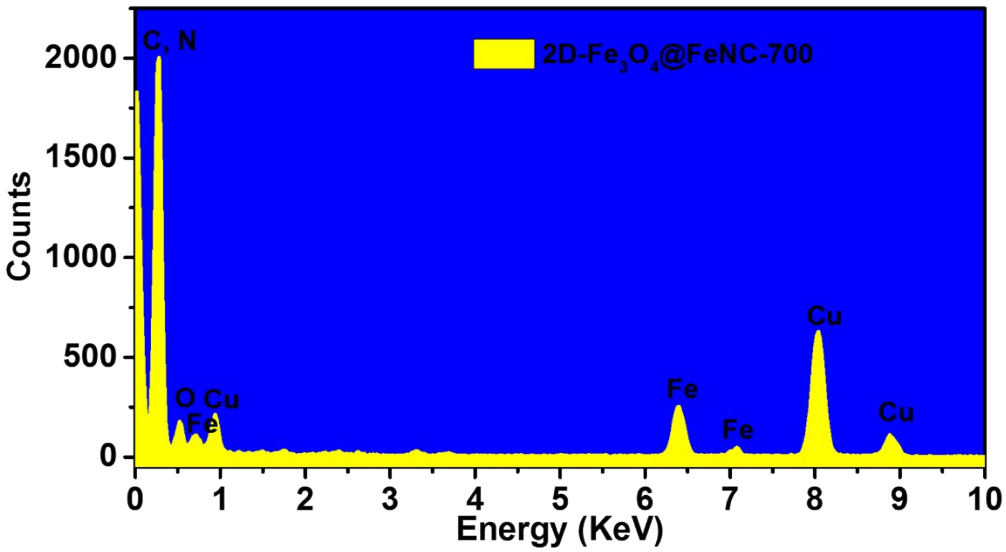

Fig. S4. EDS spectrum of 2D-Fe_3O_4@FeNC-700.

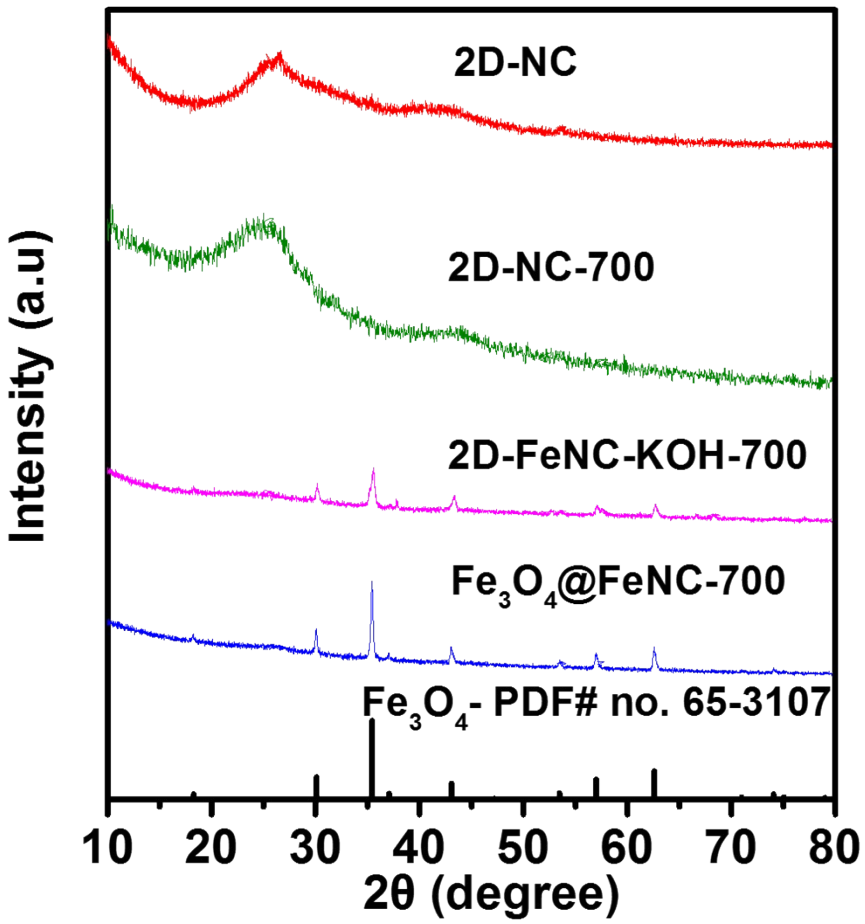

Fig. S5. Powder XRD patterns of 2D-NC, 2D-FeNC, 2D-NC-700, 2D-FeNC-KOH-700 and Fe_3O_4@FeNC-700.

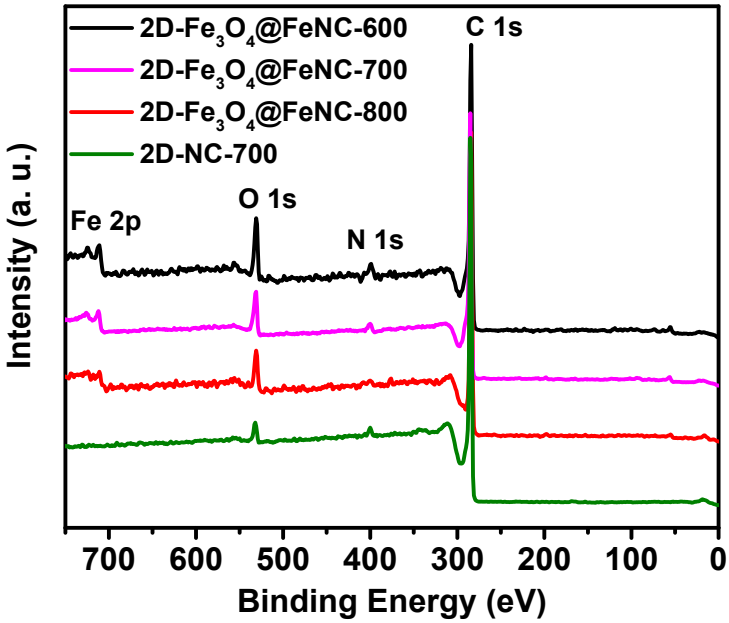

Fig. S6. XPS survey spectra of 2D-Fe_3O_4@FeNC-600, 2D-Fe_3O_4@FeNC-700, 2D-Fe_3O_4@FeNC-800 and 2D-NC-700.

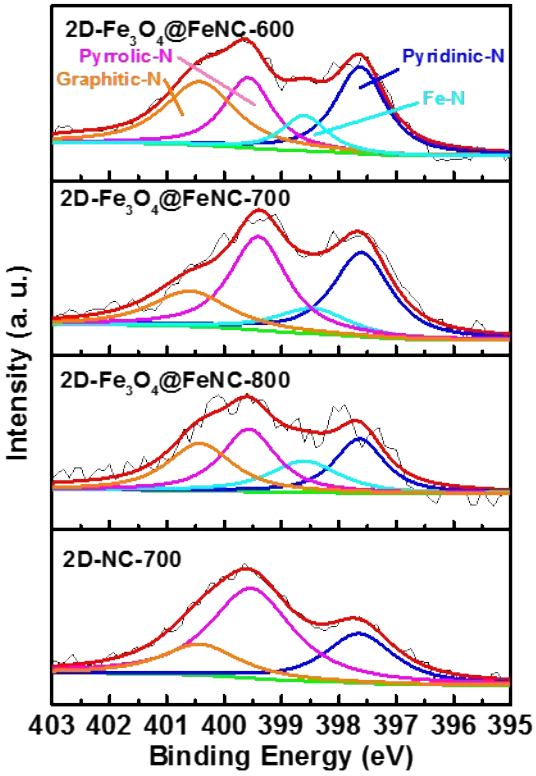

Fig. S7. High-resolution N 1s XPS spectra, and (b) high-resolution Fe 2p XPS spectra of 2D-Fe_3O_4@FeNC-*T*.

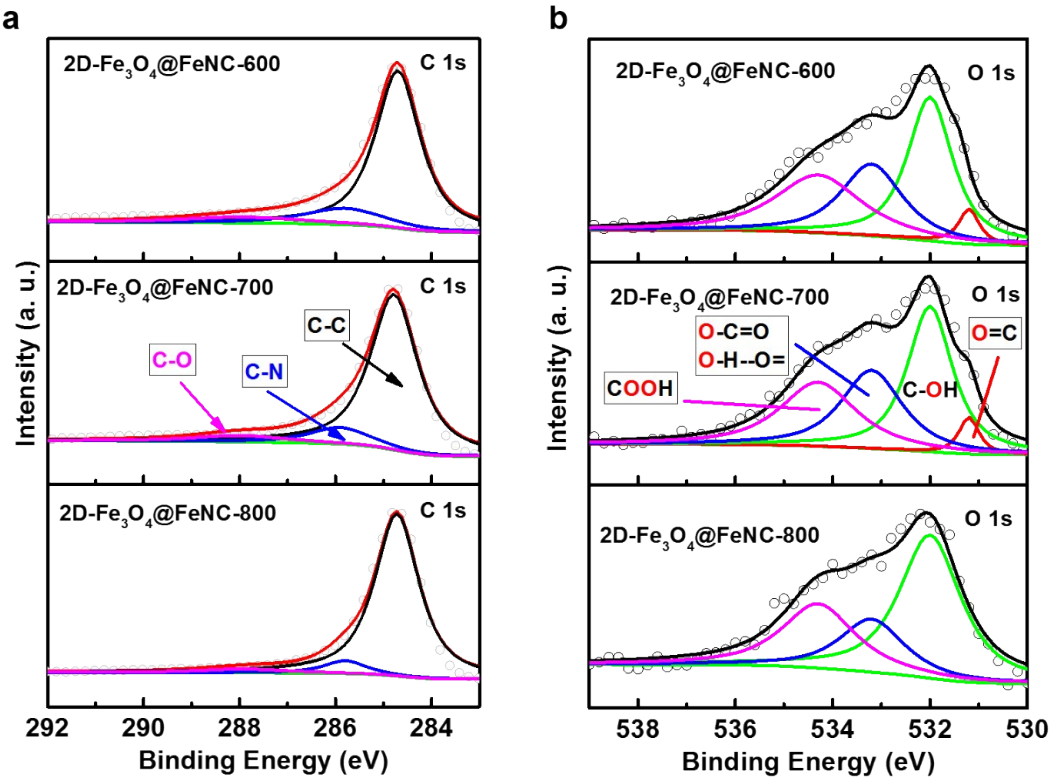

Fig. S8. High-resolution (a) C and (b) O 1s XPS spectra of 2D-Fe_3O_4@FeNC-*T*.

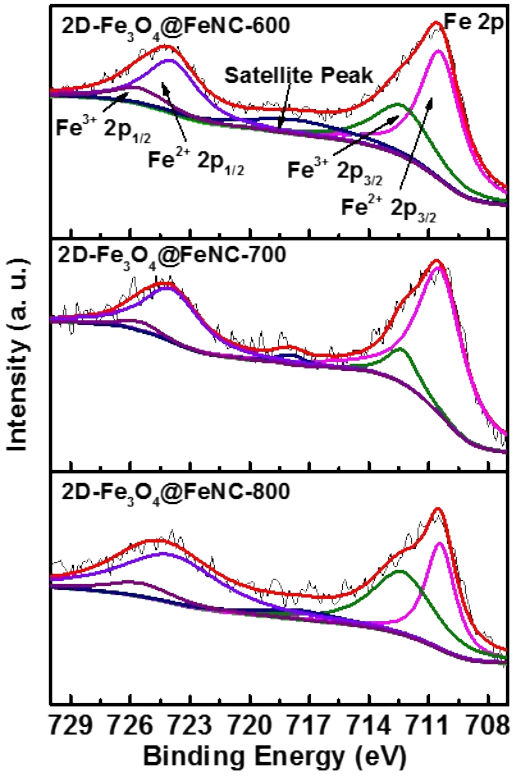

Fig. S9. High-resolution Fe 2p XPS spectra of 2D-Fe_3O_4@FeNC-*T*.

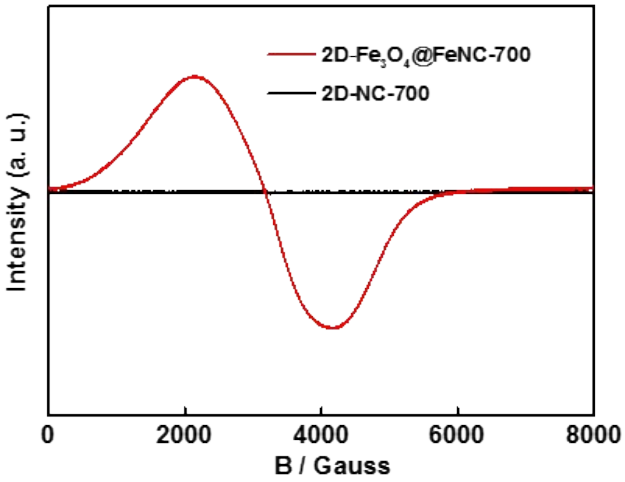

Fig. S10. X-band EPR spectra of 2D-Fe_3O_4@FeNC-700 and 2D-NC-700 catalysts under argon atmosphere at 298K.

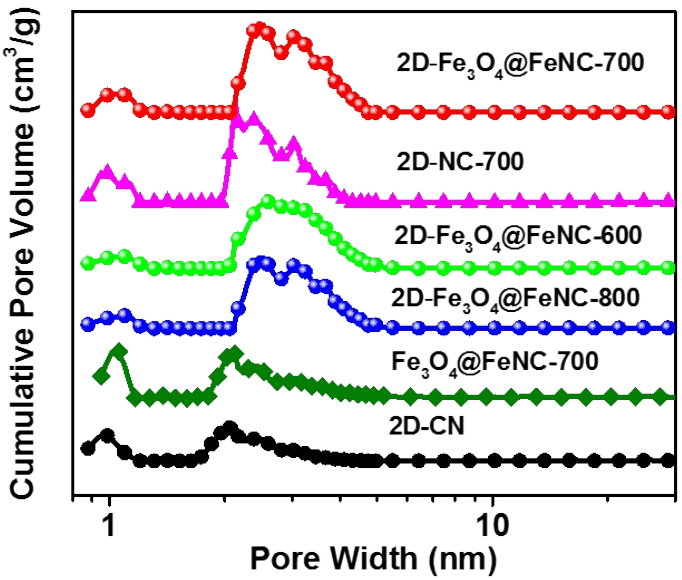

Fig. S11. The corresponding pore-size distribution curves for 2D-NC, 2D-NC-700, 2D-Fe_3O_4@FeNC-600, 2D-Fe_3O_4@FeNC-700, 2D-Fe_3O_4@FeNC-800, Fe_3O_4@FeNC-700.

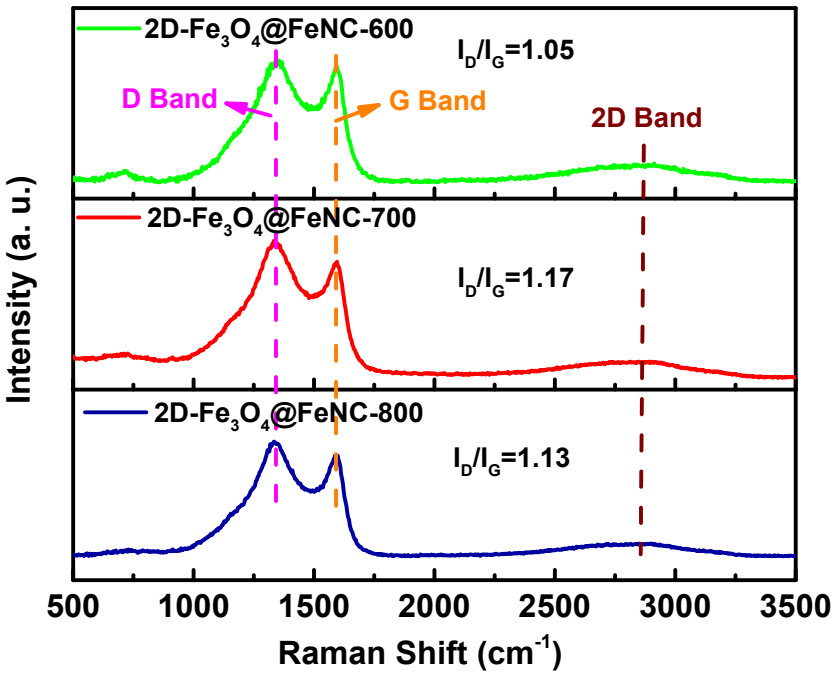

Fig. S12. Raman spectra of 2D-Fe_3O_4@FeNC-600, 2D-Fe_3O_4@FeNC-700 and 2D-Fe_3O_4@FeNC-800.

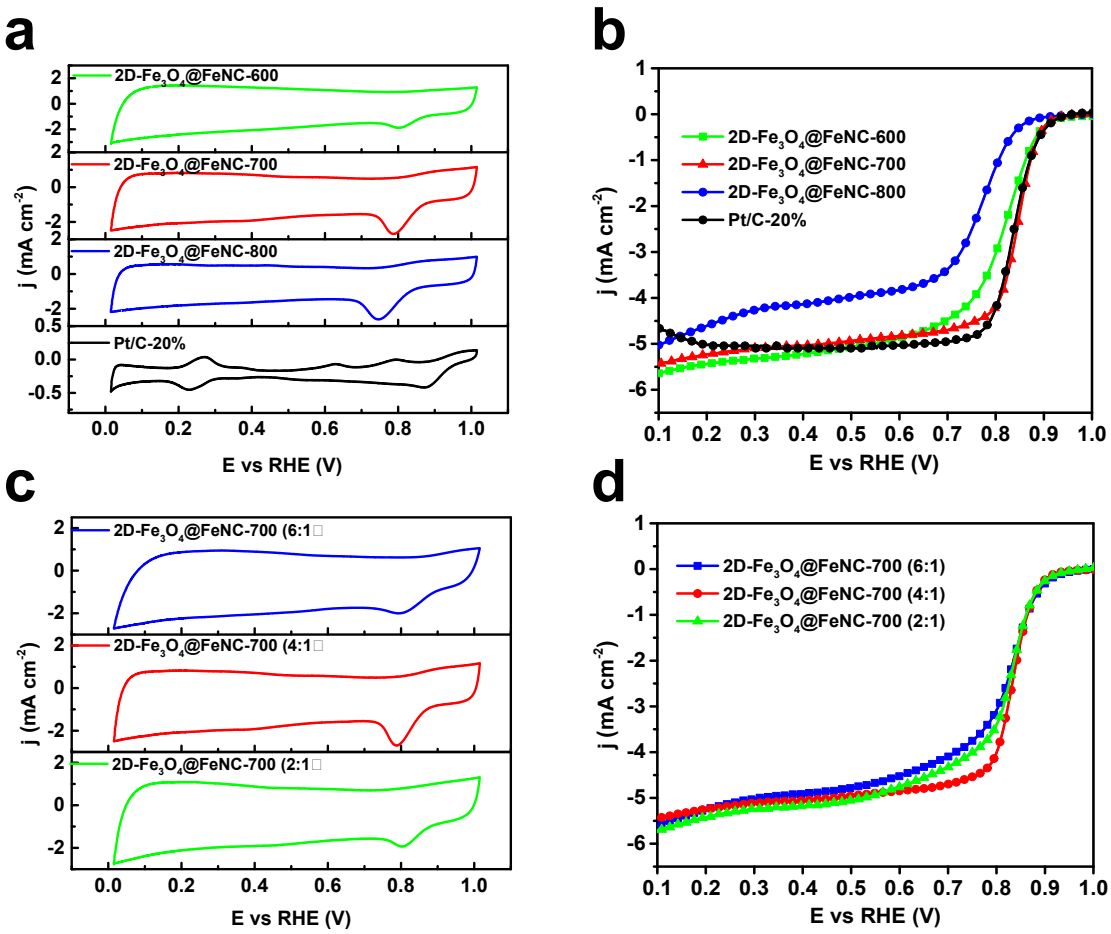

Fig. S13. (a, c) CV curves of different catalysts in O_2-saturated 0.1 M KOH at a sweep rate of 20 mVs^{-1}. (b, d) LSV polarization curves of different catalysts at 1600 rpm. 2D-Fe_3O_4@FeNC-700 (6:1), 2D-Fe_3O_4@FeNC-700 (4:1) and 2D-Fe_3O_4@FeNC-700 (2:1) were obtained via different certain concentrations of $FeCl_3$ solution (the pyrrole to $FeCl_3$ ratios of 6:1, 4:1, and 2:1).

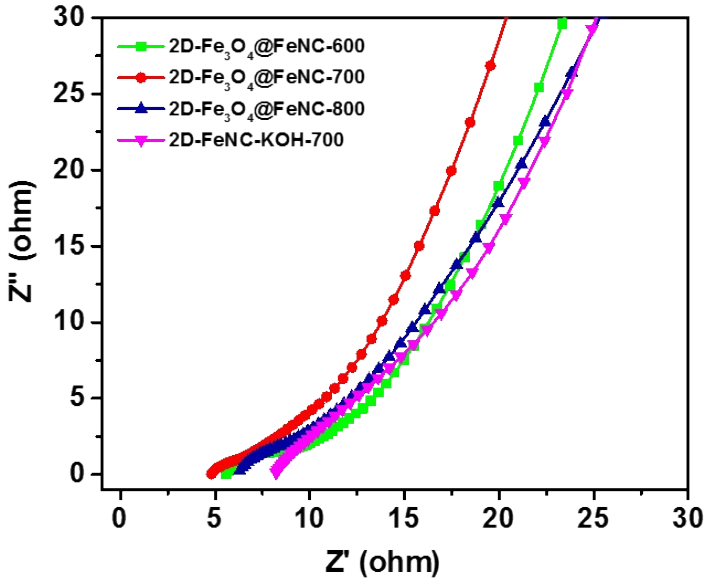

Fig. S14. Nyquist plots of 2D-Fe_3O_4@FeNC-600, 2D-Fe_3O_4@FeNC-700, 2D-Fe_3O_4@FeNC-800 and 2D-FeNC-KOH-700 recorded in O_2-saturated 0.1 M KOH aqueous.

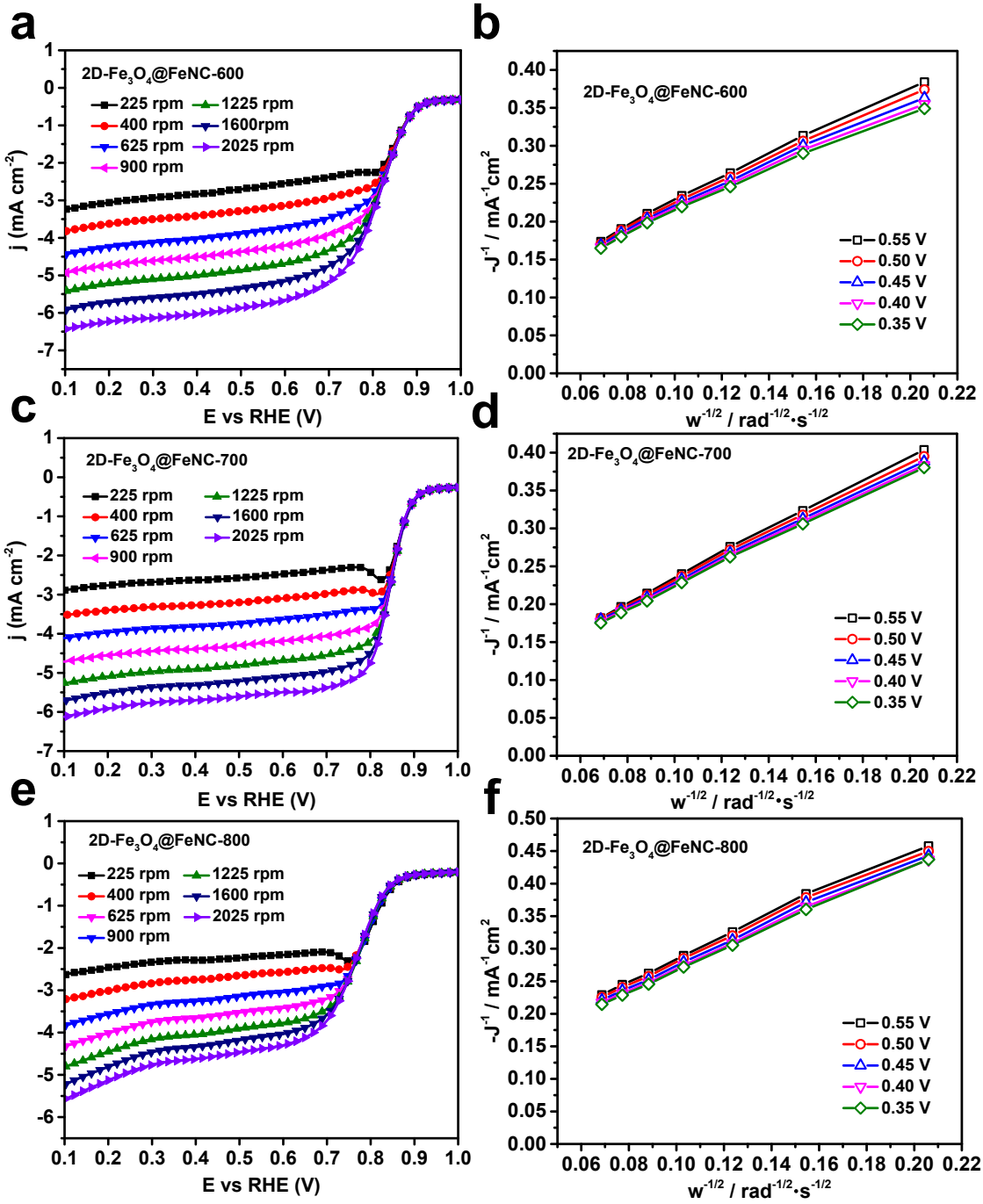

Fig. S15. (a, c, e) LSV curves at various rotational speeds (from 225 to 2025 rpm) of 2D-Fe_3O_4@FeNC-600, 2D-Fe_3O_4@FeNC-700 and 2D-Fe_3O_4@FeNC-800; and (b, d, f) the corresponding Koutechy-Levich (K-L) plots.

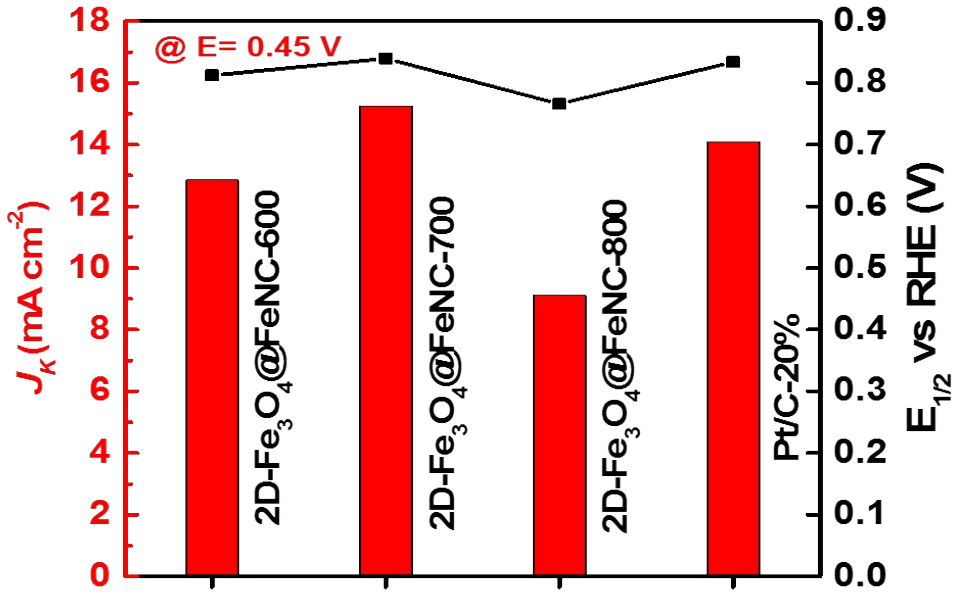

Fig. S16. Kinetic-limiting current density and $E_{1/2}$ for 2D-Fe_3O_4@FeNC-600, 2D-Fe_3O_4@FeNC-700, 2D-Fe_3O_4@FeNC-800 and Pt/C.

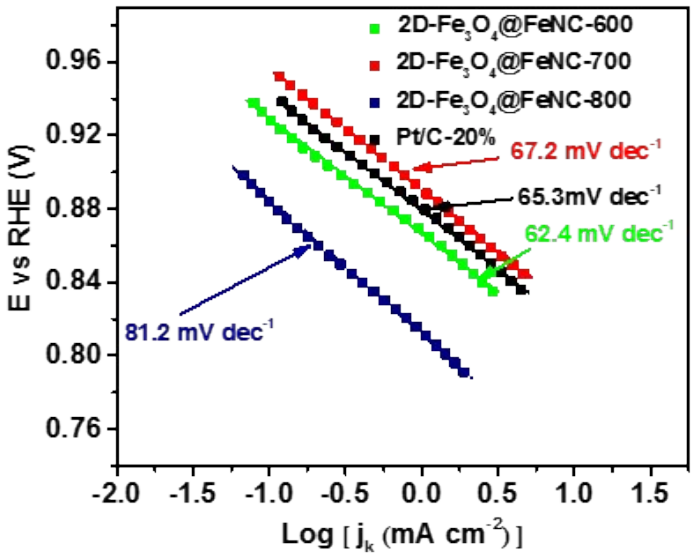

Fig. S17. Tafel plots from the corresponding LSV curves for 2D-Fe_3O_4@FeNC-600, 2D-Fe_3O_4@FeNC-700, 2D-Fe_3O_4@FeNC-800 and Pt/C.

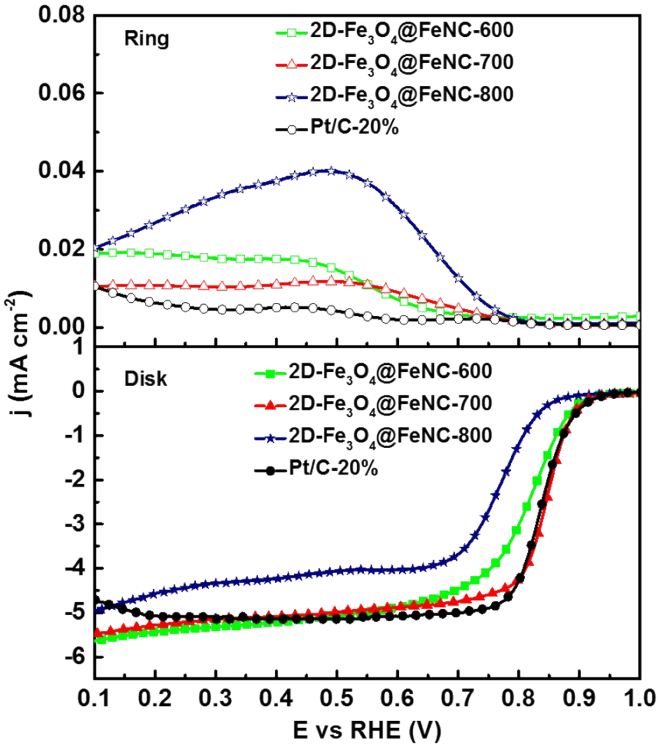

Fig. S18. RRDE curves of 2D-Fe_3O_4@FeNC-600, 2D-Fe_3O_4@FeNC-700, 2D-Fe_3O_4@FeNC-800 and Pt/C.

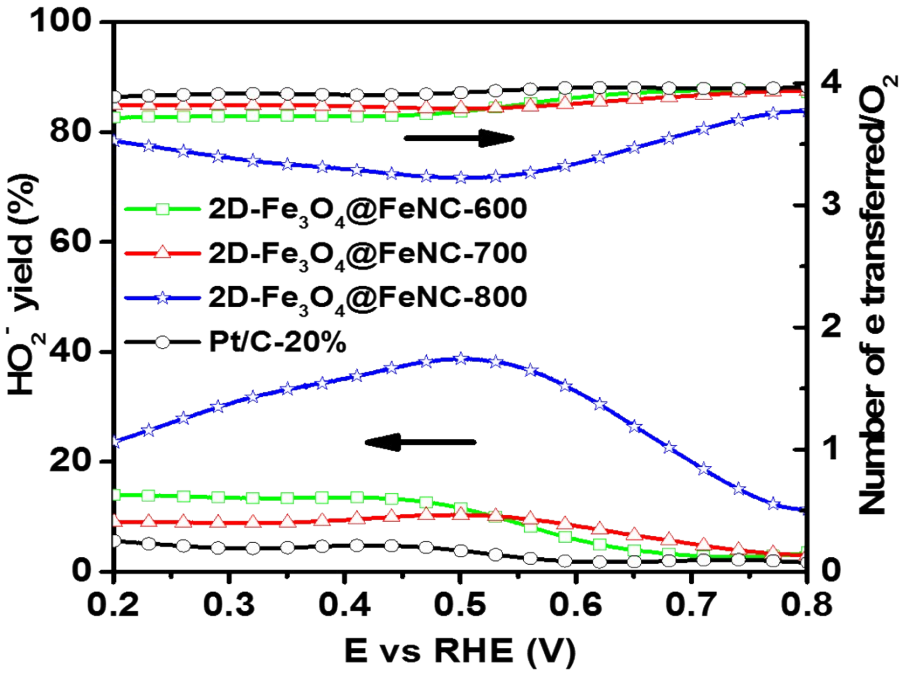

Fig. S19. Number of electrons transferred (*n*) and HO_2^- yield for 2D-Fe_3O_4@FeNC-600, 2D-Fe_3O_4@FeNC-700, 2D-Fe_3O_4@FeNC-800 and Pt/C.

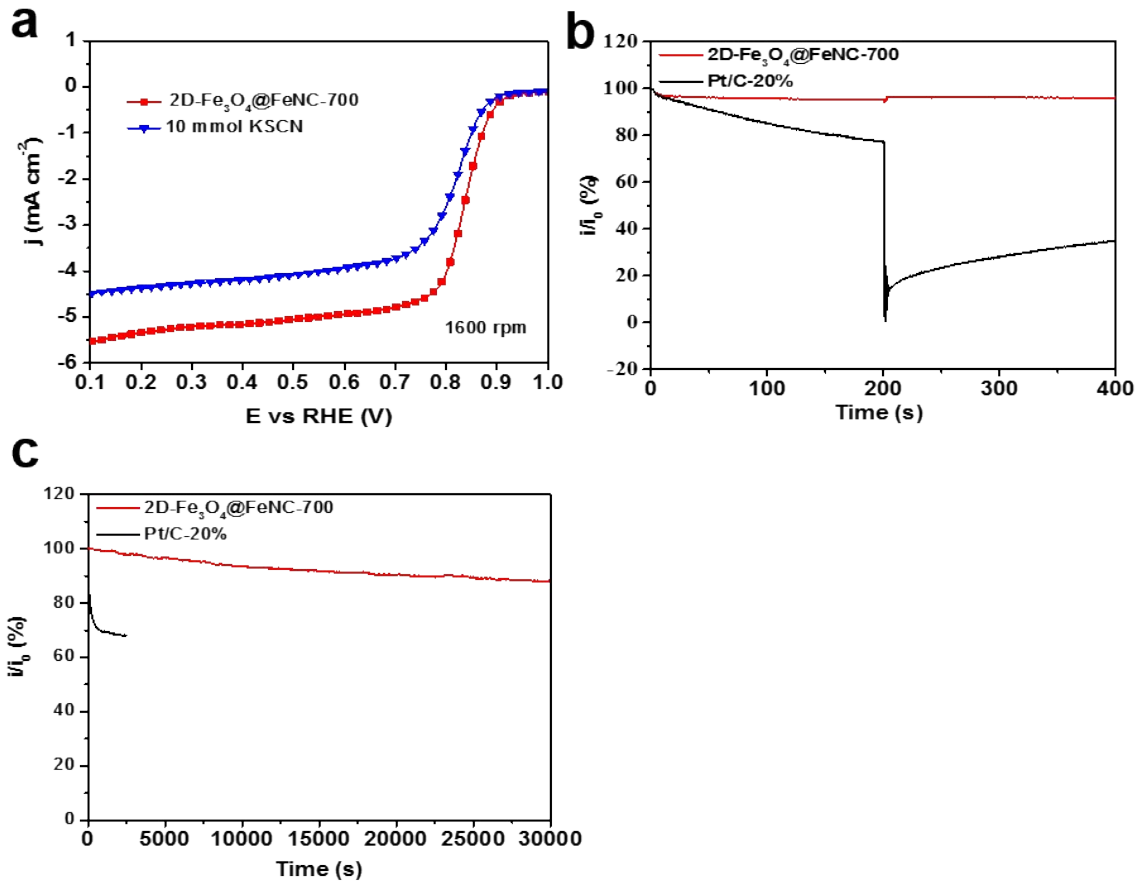

Fig. S20. (a) Effects of SCN^- ions on ORR activity of 2D-Fe_3O_4@FeNC-700. (b) Chronoamperometric response for ORR at 2D-Fe_3O_4@FeNC-700 and Pt/C with addition of 10 mL of methanol after about 200 s. (c) Long time chronoamperometric responses of 2D-Fe_3O_4@FeNC-700 and Pt/C.

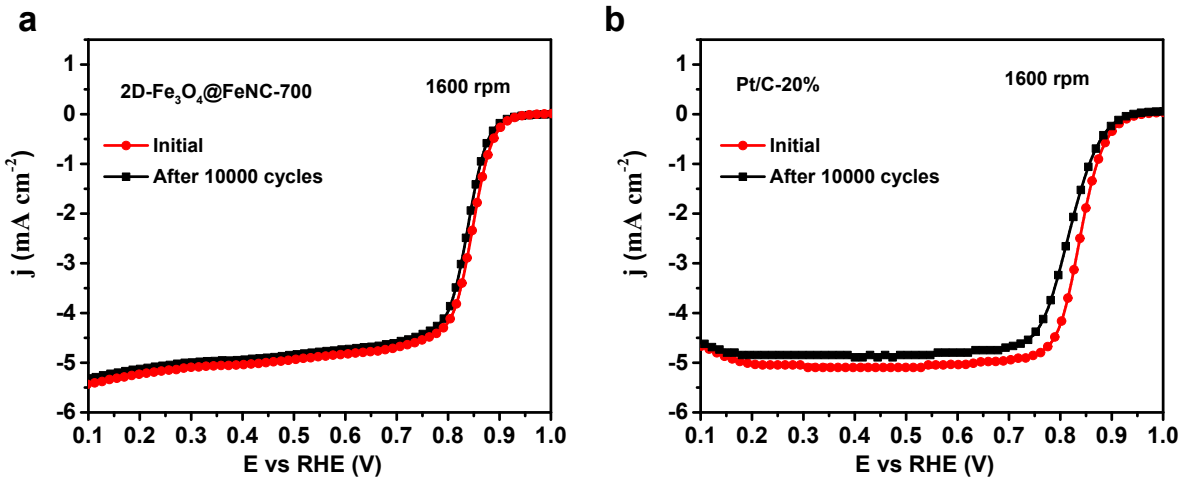

Fig. S21. LSV curves of (a) 2D-Fe_3O_4@FeNC-700 and (b) Pt/C before and after 10000 cycles by cycling the catalyst between 0.5 and 1.0 V at 50 mV s^{-1} under oxygen atmosphere.

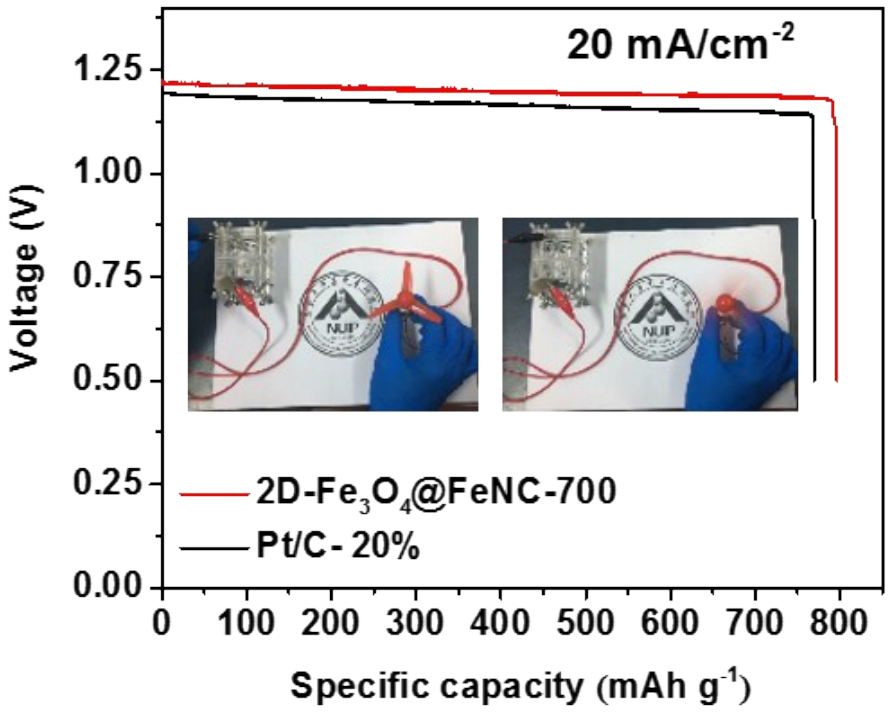

Fig. S22. Discharge curves of Zn-air batteries assembled with 2D-Fe_3O_4@FeNC-700 and Pt/C at a current density of 20 mA cm^{-2}.

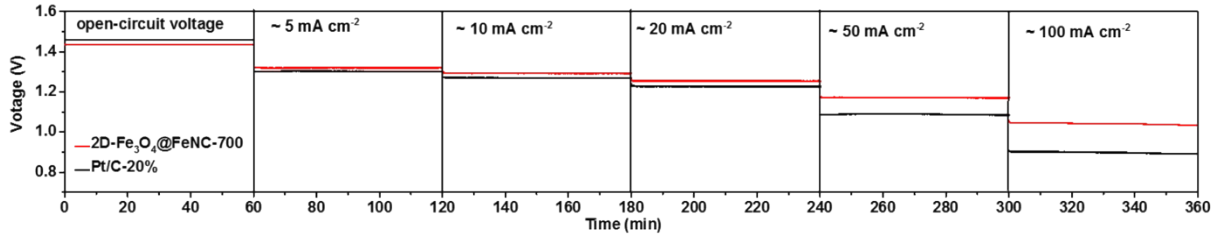

Fig. S23. Open-circuit voltage and discharge curves of the batteries under different current densities for 2D-Fe_3O_4@FeNC-700 and Pt/C.

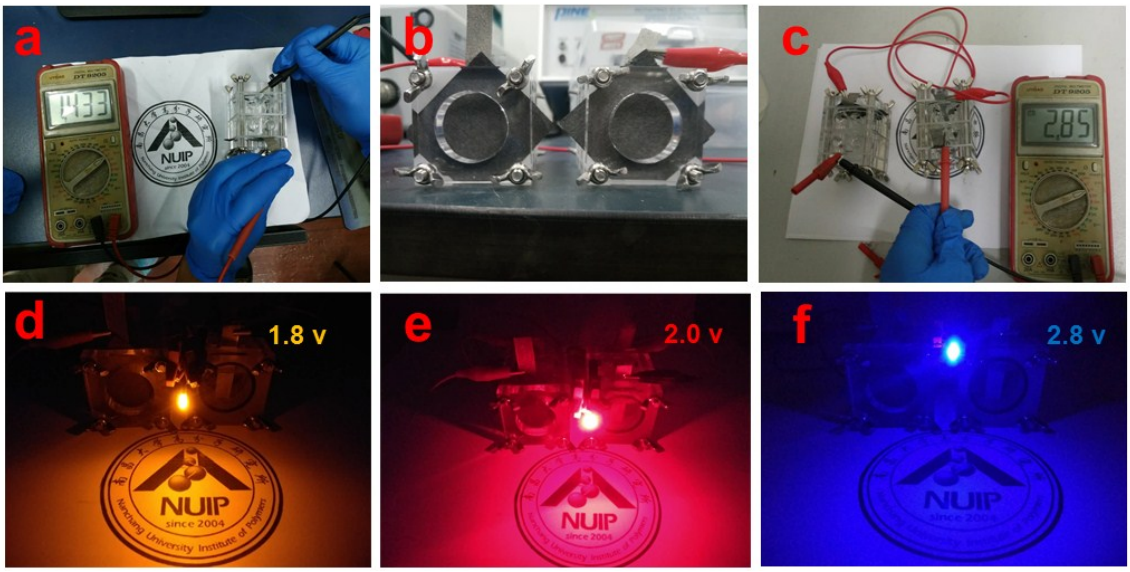

Fig. S24. (a) Open-circuit voltage of single liquid Zn-air battery assembled with 2D-Fe_3O_4@FeNC-700. (b) Photograph and (c) Open-circuit voltage of two liquid Zn-air batteries in series. (d, e, f) Photograph of a yellow LED (≈ 1.8 V), red (≈ 2.0 V), blue (≈ 2.8 V) powered by two liquid Zn-air batteries in series.

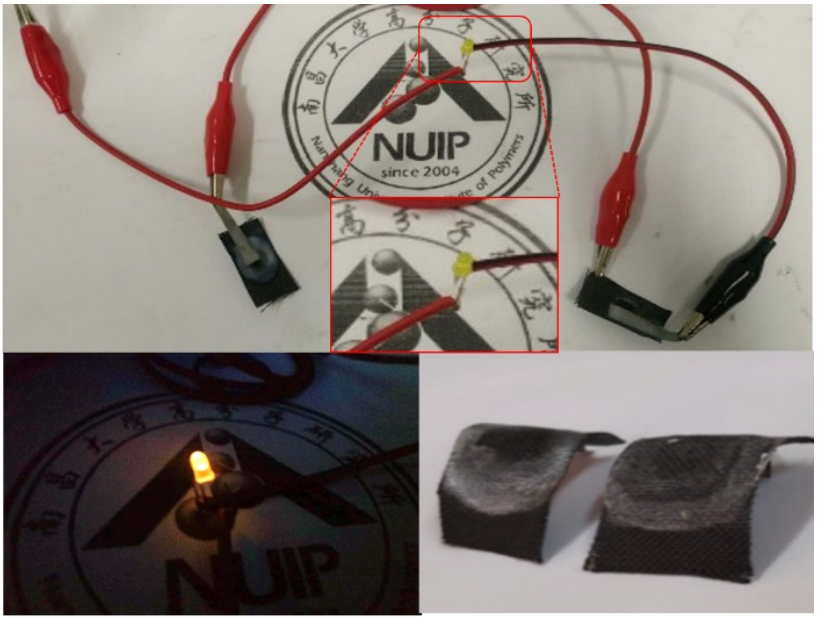

Fig. S25. Photograph single solid-state Zn-air battery (1.378 V), and two all-solid-state Zn-air batteries connected in series lighting up a yellow LED (≈ 1.8 V).

Table S1. Elemental contents of C, N, O, and Fe based on XPS analysis and energy dispersive X-ray spectroscopy (EDS) for the 2D catalysts.

Sample	Chemical composition (at %)			
	C	N	O	Fe
2D-Fe_3O_4@FeNC-600	87.28	2.15	10.57	1.73
2D-Fe_3O_4@FeNC-700	88.67	2.02	7.20	2.11
2D-Fe_3O_4@FeNC-800	92.45	1.51	4.82	1.22
2D-CN-700	95.85	1.66	2.49	-

Table S2. Summary of the Mössbauer parameters and assignment to iron species for the different Mössbauer sites.

MS site	δ_{iso} / mm s^{-1}	ΔEq / mm s^{-1}	fwhm / mm s^{-1}	H_0/T	Assignment	percentage
D1	0.46	0.73	0.36	-	Fe−N_x sites	18.9%
Sext1	0.48	-0.04	0.38	48.9	Fe_3O_4 (A)	81.1%
Sext2	0.85	0.12	0.61	44.8	Fe_3O_4 (B)	

Table S3. The Brunauer–Emmett-Teller (BET) surface area, total pore volume, and average pore width of catalysts.

Sample	BET surface area (m^2 g^{-1})	total pore volume (cm^3 g^{-1})	average pore width (nm)
2D-NC	701	0.386	2.20
2D-CN-700	1556	0.812	2.09
2D-Fe_3O_4@FeNC-700	1594	0.896	2.25
2D-Fe_3O_4@FeNC-600	1383	0.809	2.34
2D-Fe_3O_4@FeNC-800	1317	0.770	2.34
Fe_3O_4@FeNC-700	1003	0.661	2.63

Table S4. the onset potential (E_0) and half-wave potential ($E_{1/2}$) for the 2D catalysts and Pt/C.

Sample	E_0	$E_{1/2}$
2D-CN	0.784	0.653
2D-FeNC	0.895	0.762
2D-CN-700	0.824	0.716
2D-FeNC-KOH-700	0.839	0.780
Fe_3O_4@FeNC-700	0.939	0.799
2D-Fe_3O_4@FeNC-600	0.937	0.812
2D-Fe_3O_4@FeNC-700	**0.940**	**0.840**
2D-Fe_3O_4@FeNC-800	0.859	0.766
Pt/C-20%	0.942	0.834

Table S5. Comparison of ORR performance of 2D-Fe_3O_4@FeNC-700 at 1600 rpm in 0.1 M KOH with literature values.

Catalyst	Onsest potential (V vs. RHE)	Half-wave potential (V vs. RHE)	References
Fe-N/C-800	0.920	0.809	*J. Am. Chem. Soc.* **2014**, 136, 11027−11033
Fe-N-DSC	0.928	0.78	*ACS Nano* **2018**, 12, 208−216
mNC-Fe_3O_4@rGO-3	~0.93	0.813	*Small* **2018**, 14, 1702755
FeNC-800	0.959	0.815	*ACS Energy Lett*. **2018**, 3, 252−260
NC-A2	0.901	0.810	*Angew. Chem*. **2014**, 126, 9657–9661
NG-900-4	0.885	0.752	*Adv. Funct. Mater.* **2016**, 26, 5708
MF-Fe-700	0.92	0.75	*Chem. Mater*. **2017**, 29, 5617
Fe−NGM	0.93	0.72	*Chem. Mater*. **2017**, 29, 9915
Fe@Aza-PON	~0.92	0.839	*J. Am. Chem. Soc*. **2018**, 140, 1737
NFe/CNs-800	0.88	0.78	*Adv. Mater.* **2017**, 29, 1700707
Fe-N-CNFs	~0.94	0.82	*Angew. Chem. Int. Ed.* **2015**, 54, 8179
Fe@C-FeNC-1	~0.92	0.85	*J. Am. Chem. Soc*. **2016**, 138, 3570
Fe-N-C	~0.91	0.80	*Angew. Chem. Int. Ed.* **2018**, 57, 1
2D-Fe_3O_4@FeNC-700	**0.940**	**0.840**	**This Work**

Table S6. The performance of liquid Zn-air batteries with various electrocatalysts. The corresponding current densities (mA cm^{-2}) for specific capacity, peak power density and energy density are listed in the Table.

Catalyst	peak power density (mW cm^{-2})	specific capacity (mAh g^{-1})	energy density (Wh kg^{-1})	References
Ni–MnO/rGO	123	758@5	930@5	*Adv. Mater.* **2017**, 30, 1704609
$Fe_{0.5}Co_{0.5}O_x$/NrGO	86	756@10	904@10	*Adv. Mater.* **2017**, *29*, 1701410
DN-CP@G	135	591@20	~	*Adv. Energy Mater.* **2018**, 8, 1803539
Meso-CoNC@GF	154.4	~	~	*Adv. Mater.* **2018**, 30, 1704898
NGM-Co	152	750@20	840@20	*Adv. Mater.* **2017**, 29, 1703185
Co_3O_4-NP/N-rGO	118	786@5	997@5	*Adv. Energy Mater.* **2018**, 8, 1702222
Co/Co_3O_4@PGS	118.27	~	~	*Adv. Energy Mater.* **2018**, 8, 1702900
CoNCF-1000-80	170	650@10	797@10	*Small* **2018**, 14, 1703739
Fe@C–NG/NCNTs	101.3	682.6@10	764.5@10	*J. Mater. Chem. A*, **2018**, 6, 516
S,N-Fe/N/C-CNT	102.7	~	~	*Angew. Chem. Int. Ed.* **2016**, 55, 1
Fe-N/C-1/30	121.8	~	~	*Nano Energy* **2018**, 52, 29
Cu@Fe-N-C	92	~	~	*Adv. Funct. Mater.* **2018**, 28, 1802596
NKCNPs-900	131.4		889.0@4.5	*ACS Appl. Mater. Interfaces.* **2018**, 10, 29448
PBSCF-NF	127	~	~	*ACS Nano* **2017**, 11, 11594
2D-Fe_3O_4@FeNC-700	**138**	**754.5@20**	**947@20**	**This Work**